

Hydrostatic pressure and the actomyosin cortex drive mitotic cell rounding

Martin P. Stewart^{1,2}, Jonne Helenius¹, Yusuke Toyoda³, Subramanian P. Ramanathan¹, Daniel J. Muller¹ & Anthony A. Hyman³

During mitosis, adherent animal cells undergo a drastic shape change, from essentially flat to round^{1–3}. Mitotic cell rounding is thought to facilitate organization within the mitotic cell and be necessary for the geometric requirements of division^{4–7}. However, the forces that drive this shape change remain poorly understood in the presence of external impediments, such as a tissue environment². Here we use cantilevers to track cell rounding force and volume. We show that cells have an outward rounding force, which increases as cells enter mitosis. We find that this mitotic rounding force depends both on the actomyosin cytoskeleton and the cells' ability to regulate osmolarity. The rounding force itself is generated by an osmotic pressure. However, the actomyosin cortex is required to maintain this rounding force against external impediments. Instantaneous disruption of the actomyosin cortex leads to volume increase, and stimulation of actomyosin contraction leads to volume decrease. These results show that in cells, osmotic pressure is balanced by inwardly directed actomyosin cortex contraction. Thus, by locally modulating actomyosin-cortex-dependent surface tension and globally regulating osmotic pressure, cells can control their volume, shape and mechanical properties.

To analyse cell shape during mitosis, we simultaneously used atomic force microscopy (AFM), to measure cell height, and transmitted light microscopy, to measure cell width (Methods and Supplementary Fig. 1). Because we can determine the position of the cantilever with nanometre precision, this provides a similarly precise measure of the cell dimensions. Metaphase HeLa cells had a height-to-width ratio of 0.86 ± 0.04 (mean \pm s.d.; Supplementary Fig. 1b). Mitotic cells without retraction fibres were almost spherical, as were interphase cells detached with trypsin (Supplementary Fig. 1b, c). Therefore, we conclude that a detached, isolated cell will be nearly spherical, independent of its cell cycle phase. This suggests that loss of adhesion as cells enter mitosis permits cell rounding³.

A role for actin-based processes has previously been demonstrated in mitotic cell rounding^{1,4,6,8,9}. Therefore, we tested the role of the actin cytoskeleton in maintaining a spherical shape by adding cytochalasin D to rounded cells (Supplementary Fig. 1a, e). After treatment, both detached mitotic and interphase cells remained round. However, if retraction fibres were present, rounded cells sagged to height-to-width ratios of <0.5 on cytochalasin D treatment. Therefore, the actomyosin cytoskeleton is necessary for generating a rounding force against adhesion.

To quantify the force of cell rounding, a tipless cantilever was positioned over a prophase HeLa cell, 8 μm above the substrate (Fig. 1a), and held there while the cell underwent mitosis. We refer to this method as a 'constant-height assay'. When becoming rounder in prometaphase, the mitotic cell came in contact with the cantilever and the upward force that it exerted on the cantilever was measured with subnanonewton accuracy. Simultaneously, the cell's progression through mitosis was monitored using light microscopy (Fig. 1b). Within ~ 10 min after nuclear envelope breakdown, cells were cylindrical, and remained so until division. As cells progressed through

prometaphase and into metaphase, the force exerted on the cantilever increased. Because cortical tension was uniform across the cell until anaphase¹⁰ (Supplementary Fig. 2), we were able to normalize force by

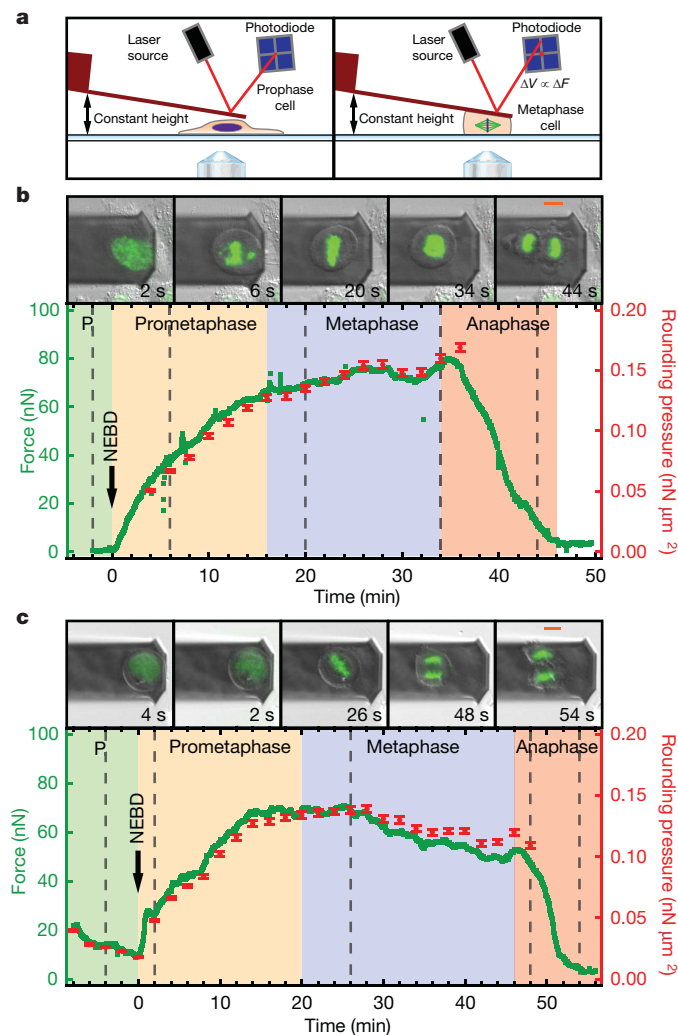


Figure 1 | Cells exert an increased rounding pressure in mitosis.

a, Constant-height assay (Methods Summary). V , voltage signal at the AFM photodiode; F , force. **b**, Overlaid differential interference contrast (DIC) and histone H2B/green fluorescent protein (GFP) images of a mitotic HeLa cell at the times indicated by the grey dashed lines. Graphed is the measured upward force (green) and calculated rounding pressure (red), which could be derived only while the cell was cylindrical (Methods). Time zero denotes nuclear envelope breakdown (NEBD). Mitotic phases are as follows: prophase (P, green), prometaphase (orange), metaphase (blue) and anaphase (red). **c**, As in **b** but for a mitotic cell pre-rounded with trypsin treatment before NEBD. Error bars, $\pm 2\%$ (based on measurement uncertainty from DIC images); scale bars, 10 μm .

¹Eth Zürich, Department of Biosystems Science and Engineering, CH-4058 Basel, Switzerland. ²Biotechnology Center, University of Technology Dresden, D-01307 Dresden, Germany. ³Max-Planck-Institute of Molecular Cell Biology and Genetics, D-1307 Dresden, Germany.

dividing it by the cross-sectional area of the cell, providing a cell 'rounding pressure'. In metaphase, the rounding pressure reached a maximum at $0.14 \pm 0.04 \text{ nN } \mu\text{m}^{-2}$ ($n = 83$). At anaphase, before ingression of the cleavage furrow, there was a transient rise in the rounding pressure. Concomitant with cytokinesis, force decreased, and the daughter cells flattened and finally lost contact with the cantilever. We also showed that individual G2/prophase cells that had been pre-rounded with trypsin and progressed into mitosis (Fig. 1c) increased their rounding pressure by more than 3-fold, despite cell size remaining relatively constant (Supplementary Fig. 3). Thus, as cells enter mitosis, they can exert considerable forces against external objects. These changes in mechanical properties resemble those of early studies on sea urchin eggs¹.

To determine what mechanisms generate the increased rounding force during mitosis, we examined the forces exerted by mitotic cells in the presence of various perturbants of the cytoskeleton. All actomyosin inhibitors tested significantly reduced the rounding pressure of mitotic cells (Fig. 2a). In contrast, perturbing microtubule dynamics increased the exerted pressure (Fig. 2a), perhaps because Rho/Rac guanine nucleotide exchange factor 2 was no longer inhibited¹². Therefore, an intact actomyosin cortex, but not the microtubule cytoskeleton, is required for rounding cells to generate a rounding pressure against an external impediment.

While performing the constant-height assay on mitotic cells using intermediate concentrations of latrunculin A (40–100 nM), we noticed oscillations in the rounding force, which correlated with blebbing (Fig. 2b). The rounding pressure decreased while blebs expanded, and recovered during bleb retraction (Fig. 2b). A bleb forms when a section of membrane detaches from the actomyosin cortex¹³ and retracts when the actomyosin cortex reassembles underneath the membrane and pulls the bleb back into the main cell body¹⁴. The concurrence of bleb formation and the decrease in rounding pressure suggests that the cell was under hydrostatic pressure: the pressure inside the cells pushing the cantilever upward was partially released when a bleb formed¹⁵. This interpretation is supported by recent measurements quantitatively relating cortical actomyosin tension with bleb formation¹⁶.

The force on the cantilever could be a result of osmotic pressure. If the osmolarity is higher inside the cell than outside, water will flow into the cell and generate a hydrostatic pressure. To test this idea, we modulated the osmolarity of the medium. Introduction of hypotonic medium ($-\Delta 100 \text{ mosM l}^{-1}$) led to an immediate increase in the volume of metaphase cells ($40 \pm 6\%$; $n = 9$), indicating that water entered the cells (Fig. 3a). This was accompanied by a concurrent increase in the measured rounding pressure ($76 \pm 20\%$; $n = 9$), presumably because the intracellular pressure increased. Within 3 min of the osmolarity changing, the cell volume and rounding pressure returned to close to their original values. This is probably because, in response to increased osmotic pressure, regulatory volume decrease causes cells to release ions¹⁷. Conversely, when hypertonic medium ($+\Delta 200 \text{ mosM l}^{-1}$) was introduced (Fig. 3b) the changes in volume ($-24 \pm 4\%$; $n = 9$) and rounding pressure ($-30 \pm 14\%$; $n = 9$) were in the opposite direction. Again, the cells recovered the original rounding pressure and volume, presumably because regulatory volume increase triggers the influx of osmolytes¹⁷.

Because ion transporters at the plasma membrane increase intracellular osmotic pressure and restore the volume of cells immediately after hypertonic challenge, we reasoned that they might also contribute to the increased rounding pressure seen in mitosis (Fig. 1). Therefore, we tested the effect of inhibiting ion transporters important in regulatory volume increase¹⁷. Among the inhibitors tested, an inhibitor of Na^+/H^+ antiporters, ethylisopropylamiloride, caused the greatest decrease in rounding pressure ($-53 \pm 10\%$; $n = 19$) and volume ($-8 \pm 2\%$; $n = 19$) (Fig. 3c). The exchange of a proton with a Na^+ ion increases the intracellular osmolarity because pH is strongly buffered in the cytoplasm; thus, a Na^+ ion has a greater effect on osmolarity than a

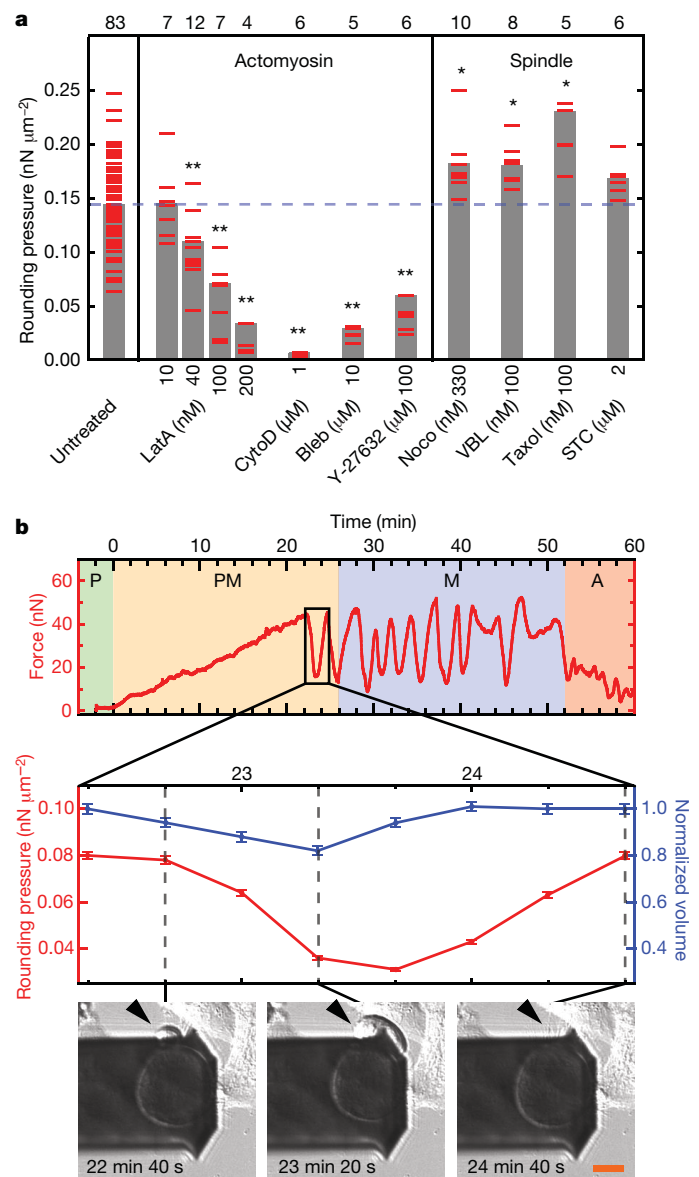


Figure 2 | Mitotic cells require a functional actin cytoskeleton to generate rounding pressure. **a**, Maximum rounding pressures generated by mitotic cells while incubated with inhibitors of the actomyosin system (latrunculin A (Lata, $n = 7, 12, 7,$ and 4 , respectively), cytochalasin D (CytoD, $n = 6$), blebbistatin (Bleb, $n = 5$), and Y-27632 ($n = 6$) or microtubule spindle perturbants (nocodazole (Noco, $n = 10$), vinblastine (VBL, $n = 8$), Taxol (TXL, $n = 5$) and S-trityl-cysteine (STC, $n = 6$)). Red marks are maximum rounding pressures generated by single cells. Grey bars denote averages. n values are shown above each category. $*P < 0.05$, $**P < 0.001$. **b**, Top: rounding force exerted by a mitotic cell incubated with 40 nM Lata. Bottom: rounding pressure (red) and cell volume (not including the bleb, blue) during an oscillation, with corresponding DIC images showing bleb expansion and retraction. The drop in rounding pressure ($< -50\%$) cannot be accounted for by the volume decrease in the main cell body ($\sim -15\%$) indicating a decrease in intracellular pressure. A, anaphase; M, metaphase; PM, prometaphase. Error bars, $\pm 2\%$ (based on measurement uncertainty from DIC images); scale bar, $10 \mu\text{m}$.

proton^{17,18}. These results suggest the Na^+/H^+ antiporter increases mitotic rounding pressure, and agree well with data showing that the Na^+/H^+ antiporter SLC9A1 is activated at the G2–M transition¹⁹.

We next perturbed the ion gradients across the plasma membrane using *Staphylococcus aureus* α -toxin, which confers permeability to monovalent cations²⁰. When added to metaphase cells, it caused a decrease in both volume ($-42 \pm 4\%$; $n = 11$) and rounding pressure

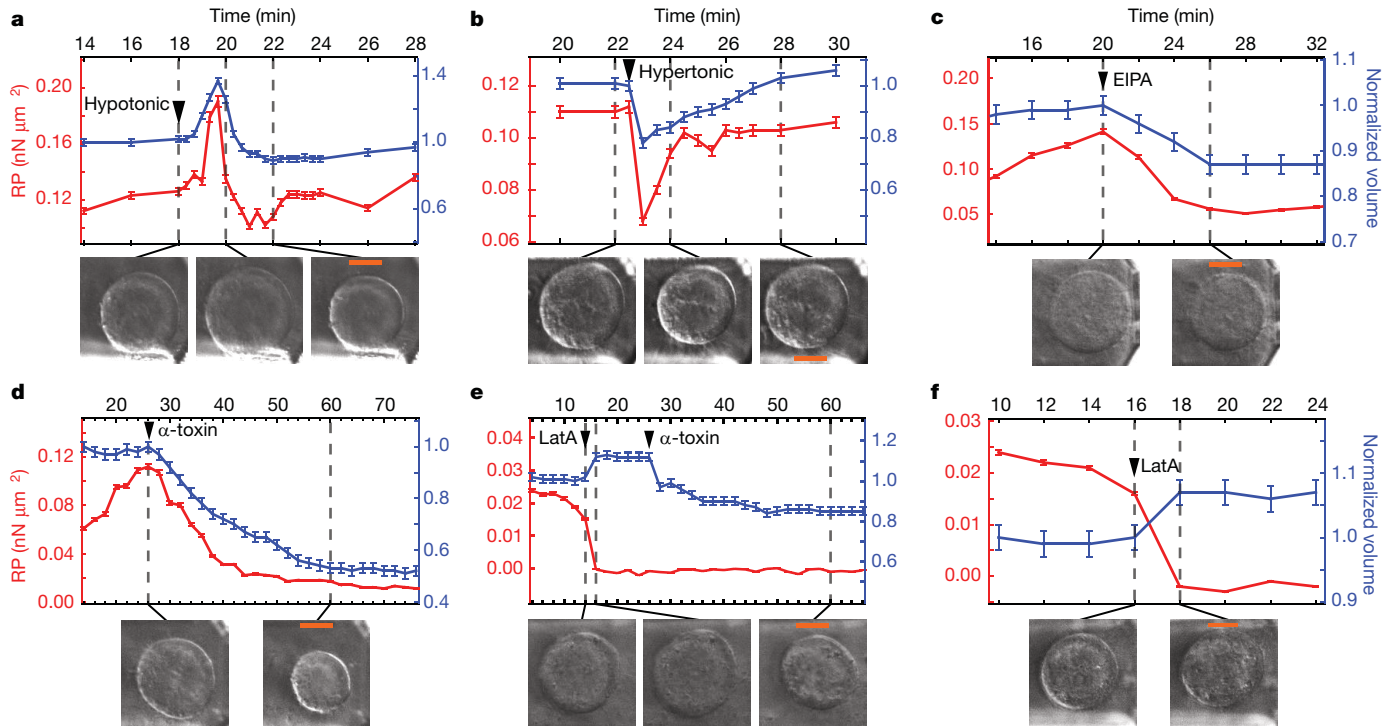


Figure 3 | The actomyosin cortex contracts against an intracellular osmotic pressure. Representative rounding pressure (RP) and cell volume time courses for mitotic cells subjected to the following perturbations: hypotonic ($-\Delta 100 \text{ mosM l}^{-1}$) medium ($n = 9$) (a); hypertonic ($+\Delta 200 \text{ mosM l}^{-1}$; +3% xylose) medium ($n = 9$) (b); 50 μM ethylisopropylamiloride (EIPA, $n = 19$)

(c); 60 $\mu\text{g ml}^{-1}$ α -toxin ($n = 11$) (d); 1 μM latrunculin A (14 min) then α -toxin (26 min, $n = 9$) (e); and 1 μM latrunculin A ($n = 36$) (f). In e and f, pre-treatment with 5 μM blebbistatin prevented latrunculin-A-induced blebbing. Time zero represents NEBD. Error bars, $\pm 2\%$ (based on measurement uncertainty from DIC images); scale bars, 10 μm .

($-88 \pm 8\%$; $n = 11$) (Fig. 3d). Another pore-forming toxin, *Escherichia coli* haemolysin A (HlyA), which also renders the plasma membrane permeable to cations²¹, also reduced the volume and rounding pressure of mitotic cells (Supplementary Fig. 4). Disruption of the actomyosin cortex with a combination of blebbistatin and latrunculin A before *S. aureus* α -toxin treatment reduced the toxin's ability to decrease cell volume (Fig. 3e), suggesting a contribution of the actomyosin cortex. We do not know whether this was due to an inward pressure caused by the actomyosin cortex or to more indirect mechanisms of volume regulation.

To further probe the link between osmotic pressure and actomyosin contraction, we performed experiments where we spontaneously abolished or stimulated the actomyosin cortex. If there is an intracellular pressure opposed by the actomyosin cortex, disruption of the cortex should result in dissipation of intracellular pressure and a small increase in cell volume. Indeed, when we treated mitotic cells first with blebbistatin, which inhibits myosin II contraction, and then with latrunculin A to depolymerize actin filaments, the volume of mitotic cells increased by $7 \pm 4\%$ ($n = 36$) and the mitotic rounding pressure was abolished (Fig. 3f). To study the converse case, we then looked at the effects of instantaneous activation of the actomyosin cortex. To do this we took advantage of blebbistatin's propensity to be inactivated by blue light²². When we photoinactivated blebbistatin, mitotic cells responded with an increase in rounding pressure and a decrease in volume (Supplementary Fig. 5). We conclude that stimulating contraction of the actomyosin cytoskeleton increases rounding pressure and decreases volume, whereas disrupting actomyosin activity reduces rounding pressure and increases volume.

Our experiments show that perturbation of osmotic gradients, associated transporters and the actomyosin cortex caused changes in both volume and rounding pressure (Fig. 4). When osmotic pressure was reduced, rounding pressure and volume decreased (Fig. 4a,

b, lower left quadrants). Conversely, if osmotic pressure was increased, rounding pressure and volume increased (Fig. 4a, b, upper right quadrants). When the actomyosin cytoskeleton was abolished, cell volume increased while rounding pressure decreased (Fig. 4a, b, lower right quadrants). However, rounding pressure increased as volume decreased after actomyosin contraction was stimulated (Fig. 4a, b, upper left quadrants). In conclusion, these results reveal that the actomyosin cortex contracts against an opposing intracellular osmotic pressure.

We propose the following model for the active processes that drive cell rounding during mitosis. As cells enter mitosis, de-adhesion from the substrate allows cells to become rounder³ (Supplementary Fig. 1). At the same time, cells increase their intracellular pressure (Fig. 1), presumably to drive rounding in a tightly packed tissue environment. Our model implies that intracellular pressure is at least equal to the measured rounding pressure, $\sim 150 \text{ Pa}$ ($0.15 \text{ nN } \mu\text{m}^{-2}$; Fig. 1). A pressure difference across the cell membrane of 100–500 Pa is thought to be sufficient to cause cell blebbing¹⁵ and is within the range typically measured in micropipette aspiration techniques²³ (1–1,000 Pa). A corollary to this model is that a non-homogeneous cortex results in dissimilar cell surface curvatures such as those observed in blebbing cells. In conjunction with an intracellular hydrostatic pressure, local modulation of cortical tension would allow cells to alter their shape^{24,25}, control their motion^{25–29} and govern the mechanics of mitosis¹⁵.

Pressure gradients are known to drive shape changes in organisms with cell walls³⁰. Our experiments support the idea that the actomyosin cortex behaves like an internal cell wall that directs osmotic expansion to control animal cell shape^{25–29}. Given the intricate shapes microorganisms and plants are able to achieve using turgor pressure, it is perhaps not surprising that animal cells have also evolved a mechanism that makes use of osmotic pressure.

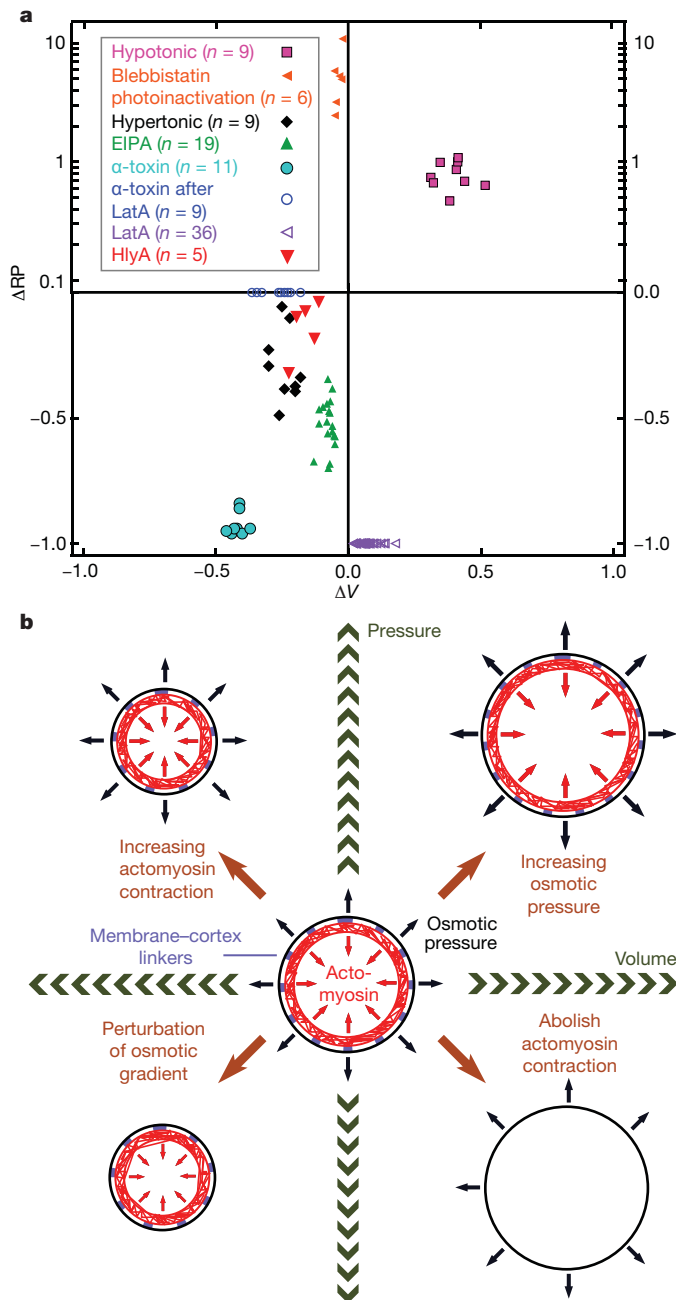


Figure 4 | Animal cells control shape in mitosis by modulating intracellular pressure in conjunction with actomyosin activity. **a**, Relative maximum changes in rounding pressure (ΔRP) and normalized volume (ΔV) of mitotic cells upon treatment with the indicated perturbations. Concentrations used are those indicated in Fig. 3 legend, $2 \mu\text{g ml}^{-1}$ for haemolysin A (HlyA) and $10 \mu\text{M}$ for blebbistatin photoinactivation, which involved a 1-s exposure to blue light. ΔRP is shown on a logarithmic scale above $\Delta RP = 0.1$. n values are displayed in the key. **b**, Uniform actomyosin contractile tension (red) is balanced by an outward-directed, intracellular osmotic pressure (black). Membrane-cortex linkers (purple) couple these two elements. The higher the tension and pressure, the greater the cortex rigidity. Imbalances between tension and osmotic pressure cause changes in cell volume and rounding force.

METHODS SUMMARY

Cell culture. HeLa-Kyoto cells expressing a fluorescent histone construct (H2B-GFP) were grown to ~50% confluency on 24-mm-diameter glass coverslips for cantilever experiments. We used DMEM containing 4 mM sodium bicarbonate (PN:31600-083, Invitrogen) buffered with 20 mM HEPES for experiments.

Instrumentation. The experimental set-up consisted of an AFM (Nanowizard I, JPK Instruments) mounted on a Zeiss Axiovert 200M optical microscope. Tipless

cantilevers were ~250 μm long, 35 μm wide, 2 μm thick and made of pure silicon (NSC12-D/tipless/noAl, $k \approx 0.3 \text{ N m}^{-1}$, Mikromasch). A BioCell (JPK Instruments) maintained cells at 37 °C.

AFM constant-height assay. We positioned the end of the cantilever over a candidate cell, 8 μm above the substrate. A laser beam was used to monitor the position of the cantilever, which was calibrated and used to record forces generated by cells. Rounding pressure was derived by dividing the measured force by the horizontal cross-sectional area of the cell, which was measured using DIC images. Cell volume was determined by multiplying the cross-sectional area of the near-cylindrical cell by its height under the cantilever. The $\pm 2\%$ error in rounding pressure and volume shown in the figures is based on measurement uncertainty from DIC images.

In Fig. 2a, cells were pre-incubated with perturbants. In Fig 3a, b, tonic shock was induced by exchanging the full volume of the AFM BioCell several times with WPI Aladdin push-pull pumps. In Fig. 3c–f, perturbants were added to the AFM BioCell with a microsyringe.

We determined the following mitotic phases from H2B-GFP images: prophase, condensed chromosomes but intact nucleus; prometaphase, nuclear envelope breakdown; metaphase, chromosomes aligned to form a metaphase plate; anaphase, two sets of chromosomes separated.

Full Methods and any associated references are available in the online version of the paper at www.nature.com/nature.

Received 11 November 2009; accepted 1 November 2010.

Published online 2 January 2011.

- Cramer, L. P. & Mitchison, T. J. Investigation of the mechanism of retraction of the cell margin and rearward flow of nodules during mitotic cell rounding. *Mol. Biol. Cell* **8**, 109–119 (1997).
- Gibson, M. C., Patel, A. B., Nagpal, R. & Perrimon, N. The emergence of geometric order in proliferating metazoan epithelia. *Nature* **442**, 1038–1041 (2006).
- Harris, A. Location of cellular adhesions to solid substrata. *Dev. Biol.* **35**, 97–114 (1973).
- Carreno, S. *et al.* Moesin and its activating kinase Slik are required for cortical stability and microtubule organization in mitotic cells. *J. Cell Biol.* **180**, 739–746 (2008).
- Kunda, P. & Baum, B. The actin cytoskeleton in spindle assembly and positioning. *Trends Cell Biol.* **19**, 174–179 (2009).
- Kunda, P., Pelling, A. E., Liu, T. & Baum, B. Moesin controls cortical rigidity, cell rounding, and spindle morphogenesis during mitosis. *Curr. Biol.* **18**, 91–101 (2008).
- Théry, M. & Bornens, M. Cell shape and cell division. *Curr. Opin. Cell Biol.* **18**, 648–657 (2006).
- Fujibuchi, T. *et al.* AIP1/WDR1 supports mitotic cell rounding. *Biochem. Biophys. Res. Commun.* **327**, 268–275 (2005).
- Maddox, A. S. & Burridge, K. RhoA is required for cortical retraction and rigidity during mitotic cell rounding. *J. Cell Biol.* **160**, 255–265 (2003).
- Matzke, R., Jacobson, K. & Radmacher, M. Direct, high-resolution measurement of furrow stiffening during division of adherent cells. *Nature Cell Biol.* **3**, 607–610 (2001).
- Hiramoto, Y. Mechanical properties of sea urchin eggs. I. Surface force and elastic modulus of the cell membrane. *Exp. Cell Res.* **32**, 59–75 (1963).
- Krendel, M., Zenke, F. T. & Bokoch, G. M. Nucleotide exchange factor GEF-H1 mediates cross-talk between microtubules and the actin cytoskeleton. *Nature Cell Biol.* **4**, 294–301 (2002).
- Cunningham, C. C. Actin polymerization and intracellular solvent flow in cell surface blebbing. *J. Cell Biol.* **129**, 1589–1599 (1995).
- Charras, G. T., Hu, C. K., Coughlin, M. & Mitchison, T. J. Reassembly of contractile actin cortex in cell blebs. *J. Cell Biol.* **175**, 477–490 (2006).
- Charras, G. T., Coughlin, M., Mitchison, T. J. & Mahadevan, L. Life and times of a cellular bleb. *Biophys. J.* **94**, 1836–1853 (2008).
- Tinevez, J. Y. *et al.* Role of cortical tension in bleb growth. *Proc. Natl Acad. Sci. USA* **106**, 18581–18586 (2009).
- Lang, F. *Mechanisms and Significance of Cell Volume Regulation* (Karger, 2006).
- Wehner, F., Olsen, H., Tinel, H., Kinne-Saffran, E. & Kinne, R. K. Cell volume regulation: osmolytes, osmolyte transport, and signal transduction. *Rev. Physiol. Biochem. Pharmacol.* **148**, 1–80 (2003).
- Putney, L. K. & Barber, D. L. Na-H exchange-dependent increase in intracellular pH times G2/M entry and transition. *J. Biol. Chem.* **278**, 44645–44649 (2003).
- Valeva, A. *et al.* Staphylococcal alpha-toxin: repair of a calcium-impermeable pore in the target cell membrane. *Mol. Microbiol.* **36**, 467–476 (2000).
- Koschinski, A. *et al.* Why *Escherichia coli* alpha-hemolysin induces calcium oscillations in mammalian cells—the pore is on its own. *FASEB J.* **20**, 973–975 (2006).
- Kolega, J. Phototoxicity and photoinactivation of blebbistatin in UV and visible light. *Biochem. Biophys. Res. Commun.* **320**, 1020–1025 (2004).
- Hochmuth, R. M. Micropipette aspiration of living cells. *J. Biomech.* **33**, 15–22 (2000).
- Salbreux, G., Joanny, J. F., Prost, J. & Pullarkat, P. Shape oscillations of non-adhering fibroblast cells. *Phys. Biol.* **4**, 268–284 (2007).

25. Blaser, H. *et al.* Migration of zebrafish primordial germ cells: a role for myosin contraction and cytoplasmic flow. *Dev. Cell* **11**, 613–627 (2006).
26. Bereiter-Hahn, J. Mechanics of crawling cells. *Med. Eng. Phys.* **27**, 743–753 (2005).
27. Charras, G. & Paluch, E. Blebs lead the way: how to migrate without lamellipodia. *Nature Rev. Mol. Cell Biol.* **9**, 730–736 (2008).
28. Mitchison, T. J., Charras, G. T. & Mahadevan, L. Implications of a poroelastic cytoplasm for the dynamics of animal cell shape. *Semin. Cell. Dev. Biol.* **19**, 215–223 (2008).
29. Keren, K., Yam, P. T., Kinkhabwala, A., Mogilner, A. & Theriot, J. A. Intracellular fluid flow in rapidly moving cells. *Nature Cell Biol.* **11**, 1219–1224 (2009).
30. Harold, F. M. To shape a cell: an inquiry into the causes of morphogenesis of microorganisms. *Microbiol. Rev.* **54**, 381–431 (1990).

Supplementary Information is linked to the online version of the paper at www.nature.com/nature.

Acknowledgements DFG, BMBF and SNF supported this project. JSPS supported Y.T. A.A.H. is funded by the Max Planck Society. We thank S. Bhakdi for toxins and advice on

their use, T. J. Mitchison for extensive discussions on osmotic pressure and critical reading of the manuscript, M. Krieg for valuable insights into cell blebbing, and B. Baum, C. Brangwynne, S. Grill, A. Helenius, J. Howard, F. Jülicher, Z. Maliga and E. Paluch for discussions and critical reading of the manuscript.

Author Contributions M.P.S., D.J.M., Y.T. and A.A.H. designed and implemented the assay. M.P.S. performed the experiments except for the Young's modulus measurements, which were made by J.H. S.P.R. contributed to Fig. 2 and Supplementary Fig. 6. Y.T. produced cell lines. J.H. designed the toxin experiments. M.P.S. analysed data and created the figures. M.P.S., J.H., D.J.M. and A.A.H. wrote the manuscript.

Author Information Reprints and permissions information is available at www.nature.com/reprints. The authors declare no competing financial interests. Readers are welcome to comment on the online version of this article at www.nature.com/nature. Correspondence and requests for materials should be addressed to A.A.H. (hyman@mpi-cbg) or D.J.M. (daniel.muller@bsse.ethz.ch).

METHODS

Cell culture. HeLa-Kyoto cells expressing a histone H2B-eGFP construct (H2B-GFP) were used³¹. In some experiments, cells additionally expressing mCherry-CAAX, fluorescently marking the plasma membrane, were used. To construct the mCherry-CAAX plasmid (TH0477), a DNA sequence (5'-TGCATGAGCTGC AAGTGTGTGCTGTCC-3') from the carboxy terminus of the rat c-H-Ras 1 gene was inserted to the C terminus of the mCherry gene³². The mCherry-CAAX plasmid was transfected into H2B-GFP cells and selected by puromycin resistance. Cells were maintained in DMEM supplemented with 10% fetal bovine serum (FBS), 2 mM GlutaMAX, 100 units ml⁻¹ penicillin, 100 µg ml⁻¹ streptomycin and 0.5 mg ml⁻¹ Geneticin (all Invitrogen) at 37 °C in a 5% CO₂ environment. DMEM used for AFM experiments (cat. no. 31600-083, Invitrogen) contained only 4 mM sodium bicarbonate and was instead buffered with 20 mM HEPES/NaOH to pH 7.2. When using dynasore and trypsin, NuSerum (Fischer Scientific) was substituted for FBS at the corresponding concentration. For AFM experiments, cells were plated on 24-mm-diameter glass coverslips (Marienfeld) and grown for 2 days until they reached ~50% confluency.

Perturbants. Chemical inhibitors were acquired from Sigma-Aldrich except jasplakinolide (Merck) and trypsin (Invitrogen) and used at the indicated concentrations. In cases where perturbants were added during a measurement, a microsyringe (Hamilton) was used to inject agents into the AFM BioCell or the full volume was exchanged several times with a WPI Aladdin push-pull pump set-up (Supplementary Fig. 7a). Supplementary Table 1 lists all perturbants used and how they were added to cells, and provides a short description of what the perturbant does.

Pore-forming-toxin experiments. *S. aureus* α -toxin stock was made at 2 mg ml⁻¹ in PBS. Owing to having limited amounts of toxin stock, we added 100 µl of a $\times 5$ concentrate to 400 µl of medium to arrive at the final concentration. Concentrate was added with a tube and syringe in the manner shown in Supplementary Fig. 7a. At a given concentration of α -toxin, more crowded coverslips seemed to dilute the potency of the toxin. Thus, for toxin experiments we attempted to keep the cell confluency constant at 40–50%. Concentrations at and below 20 µg ml⁻¹ had no noticeable effect on cells. We found a dosage of 40–80 µg ml⁻¹ caused effects such as those seen in Fig. 3d.

Haemolysis A stock was made up at 910 µg ml⁻¹ in 8 M guanine/HCl solution. Again, owing to having limited amounts of toxin stock we used the $\times 5$ concentrate 'addition' method described for α -toxin. We found that a final concentration of 1 µg ml⁻¹ had little effect on cells. However, using 2–4 µg ml⁻¹ we obtained typical results seen in Supplementary Fig. 4.

Osmolarity change experiments. For osmolarity change experiments, the volume of the AFM BioCell (~400 µl) was exchanged four times at a flow rate of 2,500 µl min⁻¹ using a WPI Aladdin push-pull pump. For hypotonic exchanges, DMEM (290 mosM kg⁻¹) was diluted with water to 190 mosM kg⁻¹. In the case of hypertonic exchanges, DMEM was supplemented with xylose to increase osmolarity to 490 mosM kg⁻¹. To minimize disturbance of the AFM laser, the refractive index of all solutions was matched with Ficoll (Sigma-Aldrich), an inert sucrose polymer with negligible effect on osmolarity in solution. **Mid-experiment introduction of perturbants: balancing refractive index and osmolarity difference.** In cases where the perturbant mixture differed from the original medium in refractive index, we added Ficoll to the solution having lower refractive index until the solutions matched. 1% w/v Ficoll increased refractive index by 0.0013 with negligible change to osmolarity.

In cases where the perturbant mixture and original medium had an unintended mismatch in osmolarity, we used xylose to raise the osmolarity of the lower-osmolarity solution. 1% w/v xylose increases osmolarity by 70 mosM l⁻¹ but also increased refractive index by 0.0013. In such cases, Ficoll was additionally used to match refractive index. In all cases, Ficoll and xylose never exceeded 3% w/v and did not negatively effect progression through mitosis or the rounding forces measured.

Instrumentation. The experimental set-up consisted of an AFM (Nanowizard I, JPK Instruments) mounted on an Axiovert 200M optical microscope (Carl Zeiss). A BioCell (JPK Instruments) allowed cells to be cultured at 37 °C during experiments. Tipless cantilevers were ~250 µm long, 35 µm wide, 2 µm thick and made of pure silicon (NSC12-D/tipless/noAl from Mikromasch) and had a nominal force constant of 0.3 N m⁻¹. Cantilevers were calibrated using the thermal noise method³³.

AFM constant-height assay. The procedure for an 8-µm constant-height assay of a mitotic HeLa cell was as follows. The height of the substrate adjacent to a cell was determined. Then the cantilever end was positioned over the cell, 8 µm above the substrate. Prophase cells typically had heights of <7 µm, and were therefore initially not in contact with the cantilever. The force exerted by the rounding mitotic cell was sensed by the cantilever and recorded over time. Rounding pressure was derived by dividing the force measured by the horizontal cross-sectional

area of the cell, which was measured from DIC images of the cell (Supplementary Fig. 7c). Cell volume was determined by multiplying the cross-sectional area of the near-cylindrical cell by its height under the cantilever (Supplementary Fig. 7c). The $\pm 2\%$ error on rounding pressure and volume is based on measurement uncertainty from DIC images. After a constant-height assay, the height of the substrate was re-measured to assess mechanical drift. Experiments with more than 10% drift in relative height were discarded. Cantilever deflection drift was usually <2 nN per hour and could be neglected when considering the magnitude of forces measured.

Cell height and shape measurements. Cell heights were determined using AFM. Because the cell is soft, particularly when treated with actin perturbants, the cell height was determined by extracting a contact point from force-distance curves. As the cantilever approached the cell, a small force, of ~100–200 pN, is registered at the cantilever upon contact. The vertical distance between this contact point and the substrate was defined as the cell height. To obtain a cell height-to-width ratio, the cell's width was measured using DIC microscopy images.

Optical microscopy. For optical microscopy, a Plan Apochromat $\times 20/0.8$ objective lens (Zeiss) was used. Images were acquired with a CoolSNAP cf camera (Roper Scientific) driven by METAMORPH software (Visitron). An alternative set-up featuring an MRM camera (Zeiss) and AXIOVISION software (Zeiss) was used to acquire and analyse images in some experiments, including the ApoTome optical sectioning shown in Supplementary Fig. 7b. For H2B-GFP and mCherry-CAAX imaging, FITC and Texas red filter sets were respectively used.

Mitotic phase assignment. H2B-GFP images were used to determine the phase of mitosis according to the following criteria: prophase cells contain condensed chromosomes surrounded by a nuclear envelope; prometaphase starts with nuclear envelope breakdown; metaphase is when chromosomes align at the metaphase plate; and anaphase is when the two sets of chromosomes separate.

Cortical stiffness measurements. The measurement was made by indenting the cell cortex using a 5-µm-diameter bead glued to a NPO tipless cantilever (Veeco; nominal stiffness, 50 mN m⁻¹) with a force of 2 nN. The Young's modulus at each indentation was calculated by least-squares fitting a parabolic curve to the force-indentation curve at contact³⁴. The method was adapted from ref. 35. The bead diameter was determined using its DIC image and the cantilever spring constant was determined as described above. We assumed the cell to have a Poisson's ratio of 0.5 (ref. 35).

Constant-height assay design. We started these experiments by using soft cantilevers (Nanoworld TLL, $k \approx 50$ mN m⁻¹). However they could neither measure nor apply forces over 20 nN; therefore, we changed to stiff cantilevers. We prefer them because they allowed us to measure a wide range of forces, from tens of piconewtons to hundreds of nanonewtons. Using such cantilevers in an 8-µm constant-height assay (Supplementary Fig. 7) allowed us to sample force, rounding pressure and volume continuously. This was key to understanding perturbations where volume and pressure respond quickly (Figs 2 and 3). Additionally, we compared the effect of long-term constraint under the cantilever with measurements on a shorter timescale using a simple rheological compression assay (Supplementary Fig. 8c). We plotted our two data sets, constant-height assays ($n = 123$) and compression assays ($n = 100$), as force versus deformation (Supplementary Fig. 8a) and contact stress versus strain (Supplementary Fig. 8b). Because we get similar results whether we 'constrain the cell' or make a simple mechanical measurement on an already round one, we conclude that our constant-height assay is applicable to studying mitotic cell rounding over a broad range of deformations and timescales.

Cell viability under the cantilever. To investigate the effect of constraining cell shape in our assay on progression through mitosis, we measured the times taken for individual cells to progress from prophase to anaphase (Supplementary Fig. 9a). Cells either subjected to a constant force of 1–50 nN or constrained to a constant height of 8 µm progressed through mitosis unaffected. However, addition of cytochalasin D to cells in an 8-µm constant-height assay slightly extended the time between nuclear envelope breakdown and anaphase. Additionally, the height-to-width ratio attained by mitotic cells becoming rounder against constant forces is plotted in Supplementary Fig. 9b.

- Neumann, B. *et al.* High-throughput RNAi screening by time-lapse imaging of live human cells. *Nature Methods* **3**, 385–390 (2006).
- Ruta, M. *et al.* Nucleotide sequence of the two rat cellular rasH genes. *Mol. Cell. Biol.* **6**, 1706–1710 (1986).
- Hutter, J. L. & Bechhoefer, J. Calibration of atomic-force microscope tips. *Rev. Sci. Instrum.* **64**, 1868–1873 (1993).
- Hertz, H. Über den Kontakt elastischer Körper. *J. Reine Angew. Math.* **92**, 156–172 (1881).
- Radmacher, M., Fritz, M. & Hansma, P. K. Imaging soft samples with the atomic force microscope: gelatin in water and propanol. *Biophys. J.* **69**, 264–270 (1995).